# Aerial RIS Aided NOMA Networks with Optimized Secrecy Metrics Performance

*Faouzi TITEL [1], Mounir BELATTAR [2], Mohamed LASHAB [3], Raed ABD-ALHAMEED [4]*

[1] Dept. of Electronics, Electrical Engineering & Automation (EEA), Ecole Nationale Polytechnique de Constantine (ENPC) , LGEPC Laboratory, BP 75, A, Nouvelle ville RP, Constantine, Algeria
[2] Dept. of Electrical Engineering, 20 Août 1955 Skikda University, Laboratory of Research in Electronics (LRES), BP 26 El Hadayek, Skikda, Algeria
[3] Dept. of Electronics, Laboratory of Research LENT, University of Oum El Bouaghi, Oum El Bouaghi, Algeria
[4] Faculty of Engineering and Digital Technologies, University of Bradford, Bradford BD71 DP, United Kingdom, and Dept. of Information and Communications Engineering, Al-Farqadein University College, Basrah 61004, Iraq

f_titel@yahoo.fr , belattarmounir@yahoo.com, lashabmoh@yahoo.fr, r.a.a.abd@bradford.ac.uk

Submitted January 11, 2025 / Accepted April 1, 2025 / Online first May 6, 2025

**Abstract.** *Reconfigurable Intelligent Surface (RIS) technology is a promising technique for enhancing the performance of reconfigurable next-generation wireless networks. In this paper, we investigate the physical layer security of the downlink in RIS-aided non-orthogonal multiple access (NOMA) networks in the presence of an eavesdropper. To characterize the network performance, the expected value of the new channel statistics is derived for the reflected links in the case of Rayleigh fading distribution. Furthermore, the performance of the proposed network is evaluated in terms of the secrecy outage probability (SOP) and the strictly positive secrecy capacity (SPSC). To optimize these metrics, we employ the multi-objective artificial vultures optimization algorithm (MOAVOA), using the power allocation coefficients of the nearby and distant users as key parameters. Two case studies are considered in simulation: perfect channel state information (CSI) and imperfect CSI.*

## Keywords

Reconfigurable Intelligent Surfaces (RIS), NOMA networks, Secrecy Outage Probability (SOP), Strictly Positive Secrecy Capacity (SPSC), Multi-objective Artificial Vultures Optimization Algorithm (MOAVOA), Multi-Objective Particle Swarm Optimization (MOPSO)

## 1. Introduction

The epoch of high-speed interconnection development that characterizes the fifth generation (5G) communication networks is already arrived, while the sixth generation (6G) wireless networks era is emerging to satisfy growing necessities of massive device connectivity, efficient spectrum usage and improved security [1–4].

Consequently, in recent years, the benefits of RIS combined to NOMA have been recommended to enhance the performance of wireless communication networks [5–7]. On the one hand, NOMA is recognized as an immersive technology for 5G cellular networks and beyond. It is based on the principle of sharing the same time-frequency resources over multiple power levels. This allows more users access the network, leading to enhanced spectral efficiency and reduced latency. On the other hand, RIS is another emerging technology which has proved its potential in performance enhancement of wireless communication systems. An RIS is composed of numerous reconfigurable passive elements, where each element can induce an adjustment of amplitude and phase for the incident signal. Thus, the RIS is capable of eliminating the undesired signals and reducing the outage probability of wireless communication networks. By adjusting the amplitude-reflection coefficient and phase shift variables, coverage can be significantly enhanced [8–12].

The integration of NOMA and RIS is driven by their complementary advantages. Indeed, NOMA provides an efficient multiple access strategy in multi-user networks, improving spectral efficiency and connectivity in RIS-assisted systems. Furthermore, RISs offer several benefits to existing NOMA networks [13]. Primarily, the reflected links provided by RISs enhance the performance of existing NOMA networks by adding signal diversity without requiring extra time slots or energy. Additionally, by adjusting the phase shifts of reflecting elements and their positions, RISs can enhance or degrade the channel quality of individual users, increasing the design flexibility of NOMA networks, leading to the transition from “channel condition-based NOMA” to “quality of service (QoS)-based NOMA”. Moreover, integrating RISs in multiple-input multiple-output (MIMO) NOMA networks relaxes some strict constraints on the number of antennas at the transceivers, due to the multiple reflecting elements of the RISs.

DOI: 10.13164/re.2025.0258

Given the potential joint benefits introduced by the interplay between NOMA and RISs, the RIS-aided NOMA networks have been investigated recently. In [14], the authors examined the downlink performance of RIS-aided NOMA networks using stochastic geometry. First, they introduced a unique path loss model for RIS reflecting channels. Then, they evaluated angle distributions utilizing a Poisson cluster process (PCP) framework, which theoretically proves that the angles of incidence and reflection are uniformly distributed. Finally, they derived closed-form expressions for coverage probabilities of the paired NOMA users.

The NOMA technique can be integrated into the space-ground networks and plays an essential role in non-terrestrial communications [15–17]. RIS can be mounted on building facades, walls, and flying devices such as unmanned aerial vehicles (UAVs) and satellites in the case of non-terrestrial NOMA networks [18]. The authors in [19] investigated Low-Earth-Orbit (LEO) satellite wireless communication networks aided by RIS and NOMA to improve the spectrum efficiency and energy efficiency by suggesting a system model that includes both the line-of-sight (LoS) and non-line-of-sight (NLoS) links, and by employing successive convex approximation (SCA) to convert a non-convex problem into a convex one. In [20], the authors focused on the utilization of RIS in multi-user networks, using both orthogonal multiple access OMA and NOMA. They particularly examined the interplay between NOMA and RIS, considering whether the RIS reflection coefficients can be adjusted once or multiple times during one transmission. They distinguished between static and dynamic RIS configurations, discussing the capacity region of RIS-aided single-antenna NOMA networks and comparing it with the OMA rate region from an information-theoretic perspective, revealing that the dynamic RIS configuration is capacity achieving. Furthermore, they explored the impact of the RIS deployment location on the performance of different multiple access schemes, revealing that asymmetric and symmetric deployment strategies are preferable for NOMA and OMA, respectively.

Moreover, physical layer security (PLS) has been extensively studied for RIS-assisted NOMA networks [10, 21–23]. In [24], the authors investigated the PLS of the downlink in RIS-aided NOMA in the presence of an eavesdropper, where an RIS is deployed to enhance quality by assisting the cell-edge user in communicating with the base station (BS). They evaluated the performance of the proposed network in terms of the SOP and the average secrecy capacity (ASC). Similarly, in [25], the authors investigated the advantages of next generation wireless systems in terms of spectrum and energy efficiency by exploiting NOMA and RIS. They examined a scenario involving two legitimate users and an eavesdropper, focusing on security concerns while enabling machine-learning tools at the BS for performance enhancement. To improve security, the authors proposed a deep neural network (DNN)-based solution that allows the BS to predict performance at the destinations and adjust critical parameters, such as power allocation coefficients. They derived closed-form expressions for the SOP and analyzed the SPSC, crucial performance metrics that evaluate the system's performance against eavesdroppers.

Further considered in [26], a MOPSO algorithm was used to optimize the SOP of a downlink NOMA network supported by an RIS. The RIS assists the BS in communicating with multiple paired users, each equipped with a single antenna. A pair of non-orthogonal legitimate users consists of a proximate user and a distant user, while an eavesdropper is located behind a blockage. The authors in [27] investigated the optimization of the SOP in an RIS-aided MIMO-NOMA wireless communication system serving two users in the presence of an eavesdropper, where the CSI of the Eve is unknown to the BS. They proposed algorithms to determine the optimal RIS phase shifts, beamforming vectors, and power allocation coefficients to enhance the system’s secrecy performance.

Additionally, in [28], the authors studied the enhancement of secrecy performance in NOMA networks using multiple aerial RIS (ARIS). The study proposes deploying multiple ARIS to assist two legitimate NOMA users while multiple non-colluding eavesdroppers attempt to intercept communications. The approach combines the transmitter-user paths with the transmitter-ARIS-user paths to increase the received signal power at the legitimate users. Furthermore, the authors derived mathematical expressions for the SOPs of these NOMA-ARIS networks over Nakagami-m fading channels. They also provided asymptotic expressions for SOPs in high transmit power scenarios.

This paper emphasizes the potential of next-generation wireless systems to significantly enhance both spectral and energy efficiency by exploiting the complementary capabilities of two innovative techniques: NOMA and RIS. This is essential for supporting the demands of future networks, including ultra-dense connectivity, low-latency communication, and energy sustainability. In this work, an aerial RIS-assisted downlink NOMA network with Rayleigh fading distribution is considered. The network consists of a BS communicating with multiple paired users, aided by an RIS composed of $N$ reflective elements, in the presence of an eavesdropper. The paired users simultaneously communicate with both the BS and the RIS. However, the RIS also provides an opportunity for the eavesdropper to intercept signals transmitted from the BS, posing a security challenge. The main contribution of this work lies in the analysis and optimization of two essential security metrics: SOP and SPSC under both perfect and imperfect channel state information (CSI) scenarios. To achieve this, we employ the MOAVOA algorithm [29], a multi-objective extension of the Artificial Vultures Optimization Algorithm (AVOA), inspired by the foraging and navigation behaviors of African vultures. Specifically, MOAVOA is used to optimize the power allocation coefficients, ensuring optimal performance in terms of both security and resource efficiency.

In terms of the above details, the main related work in the paper is described as follows:

- The PLS model of an RIS-aided downlink NOMA network with Rayleigh fading distribution is formulated in the presence of two users and an eavesdropper without blockage, as seen in [26].
- The mathematical expressions of the SOP and the SPSC of the proposed RIS-aided downlink NOMA network are derived under both perfect and imperfect CSI scenarios. Moreover, the asymptotic SOP and the asymptotic SPSC in the high-SNR regime are also provided.
- A multi-objective optimization problem is formulated to determine the optimal power allocation coefficients. This approach simultaneously minimizes the SOP while maximizing the SPSC, thereby enhancing overall system security and efficiency.
- To the best of the authors' knowledge, this paper is the first to apply the Multi-Objective Artificial Vultures Optimization Algorithm to RIS-aided downlink NOMA networks for optimizing power allocation coefficients, thereby achieving optimal performance in both security and resource efficiency. Due to its heuristic and stochastic nature, this metaheuristic multi-objective optimization algorithm offers several advantages over classical methods when solving complex multi-objective problems, such as global search capability, no need for derivatives, efficient handling of nonlinear and non-convex problems, and robustness in dynamic and uncertain environments, making it ideal for wireless communication applications, including power allocation in RIS-aided NOMA networks.
- As demonstrated in [29], the MOAVOA provides very acceptable results in dealing with multi-objective optimization problems, has considerable performance in terms of both convergence and diversity and outperforms other multi-objective metaheuristic methods (MOPSO, multi-objective ant lion optimization (MOALO), multi-objective multi-verse optimization (MOMVO), genetic algorithms (MOGA), multi-objective salp swarm algorithm (MSSA) and multi-objective grey wolf optimizer (MOGWO)) regarding the generational distance (GD), inverted generational distance (IGD), maximum spread (MS), and spacing (S) indices. In this study, simulation results confirm that the MOAVOA performs better than the MOPSO algorithm for the multi-objective problem considered.
- In contrast to the approach proposed in [25], our method works without training, avoiding significant computing resources and large datasets for learning. Additionally, it effectively handles highly non-linear and constrained optimization problems with multiple conflicting objectives. Furthermore, it can find multiple optimal solutions, providing greater flexibility in decision-making.

The structure of the paper is as follows: Section 2 presents the system model analysis, while Section 3 evaluates the secrecy performance metrics. In Sec. 4, the MOAVOA algorithm is introduced to optimize the two system metrics. Section 5 provides and discusses the numerical simulation results, and finally, Section 6 concludes the study.

## 2. Analysis of System Model

In this paper, we study an RIS-assisted downlink NOMA network, where a BS communicates with multiple paired users, each equipped with a single antenna. The legitimate pair of non-orthogonal users consists of a nearby user (denoted as User 1) and a distant user (denoted as User 2) in the presence of an eavesdropper (Eve), as illustrated in Fig. 1.

In the proposed system, an RIS composed of $N$ reflective elements, positioned in a judicious location, assists the BS. User 1 can communicate with both the BS and the RIS simultaneously. However, User 2 requires the assistance of the RIS to establish communication with the BS. Additionally, the presence of the RIS creates an opportunity for the Eve to eavesdrop on messages transmitted from the BS.

The wireless channels in the RIS-NOMA system are described by Rayleigh fading model. Let $z$ represent the composite signal intended for both legitimate users, User 1 and User 2

$$z = \sqrt{Pa_1}x_1 + \sqrt{Pa_2}x_2 \tag{1}$$

where $x_1$ and $x_2$ are the transmitted signals to Users 1 and 2, while $a_1$ and $a_2$ are the power allocation coefficients for User 1 and User 2 with:

$$a_1 + a_2 = 1 \text{ and } a_1 < a_2 . \tag{2}$$

The signals received at Users 1 and 2, as well as at the eavesdropper, are affected by additive white Gaussian noise (AWGN) denoted as $n_1$, $n_2$ and $n_\mathrm{E}$, respectively, and are expressed as

$$y_1 = \left( \frac{h_\mathrm{B1}}{\sqrt{d_\mathrm{B1}^\alpha}} + \frac{\mathbf{h}_\mathrm{I1} \times \mathbf{\Phi} \times \mathbf{h}_\mathrm{BI}}{\sqrt{d_\mathrm{BI}^\alpha d_\mathrm{I1}^\alpha}} \right) z + n_1 , \tag{3}$$

$$y_2 = \left( \frac{h_\mathrm{B2}}{\sqrt{d_\mathrm{B2}^\alpha}} + \frac{\mathbf{h}_\mathrm{I2} \times \mathbf{\Phi} \times \mathbf{h}_\mathrm{BI}}{\sqrt{d_\mathrm{BI}^\alpha d_\mathrm{I2}^\alpha}} \right) z + n_2 , \tag{4}$$

$$y_\mathrm{E} = \left( \frac{h_\mathrm{BE}}{\sqrt{d_\mathrm{BE}^\alpha}} + \frac{\mathbf{h}_\mathrm{IE} \times \mathbf{\Phi} \times \mathbf{h}_\mathrm{BI}}{\sqrt{d_\mathrm{BI}^\alpha d_\mathrm{IE}^\alpha}} \right) z + n_\mathrm{E} \tag{5}$$

where $d_\mathrm{B1}$, $d_\mathrm{B2}$, $d_\mathrm{BI}$, $d_\mathrm{I1}$, $d_\mathrm{I2}$, $d_\mathrm{BE}$, $d_\mathrm{IE}$ represent the distances for the BS-User 1, BS-User 2, BS-RIS, RIS-User 1, RIS-User 2, BS-Eve and RIS-Eve links, respectively and $\alpha$ denotes the path loss exponent.

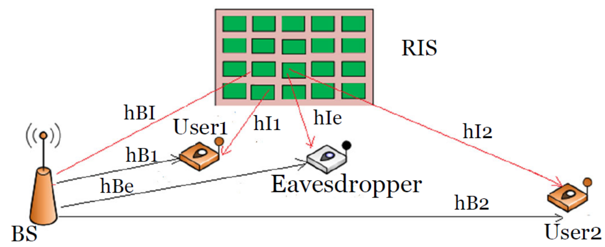


**Fig. 1.** Presentation of the system model.

The small-scale fading vector between the BS and the RIS is defined as follows

$$\mathbf{h}_{\mathrm{BI}} = \left[h_{\mathrm{BI},1}, h_{\mathrm{BI},2}, \ldots, h_{\mathrm{BI},N}\right]^{\mathrm{T}} \quad (6)$$

while the small-scale fading vectors between the RIS and the two users are denoted by

$$\mathbf{h}_{\mathrm{I1}} = \left[h_{\mathrm{I1},1}, h_{\mathrm{I1},2}, \ldots, h_{\mathrm{I1},N}\right], \quad (7)$$

$$\mathbf{h}_{\mathrm{I2}} = \left[h_{\mathrm{I2},1}, h_{\mathrm{I2},2}, \ldots, h_{\mathrm{I2},N}\right] \quad (8)$$

whereas the small-scale fading vectors between the RIS and the Eve are expressed by

$$\mathbf{h}_{\mathrm{IE}} = \left[h_{\mathrm{IE},1}, h_{\mathrm{IE},2}, \ldots, h_{\mathrm{IE},N}\right]. \quad (9)$$

Let $\mathbf{\Phi}$ a matrix defined by

$$\mathbf{\Phi} = \mathrm{diag}\left[\varphi_1 \,\mathrm{e}^{\mathrm{j}\xi_1}, \varphi_2 \,\mathrm{e}^{\mathrm{j}\xi_2}, \ldots, \varphi_N \,\mathrm{e}^{\mathrm{j}\xi_N}\right]. \quad (10)$$

Here, $0 \le \varphi_k \le 1$ and $0 \le \xi_k \le 2\pi$ for $1 \le k \le N$, represent the amplitude reflection coefficients and phase shift variables, respectively, for the $k$-th reflecting element in the RIS.

At User 1, the signal-to-noise ratio (SNR) for detecting signal $x_1$ is given by

$$\gamma_1^{x_1} = \rho a_1 \psi_1 . \quad (11)$$

The expression of $\psi_1$ in the case of imperfect CSI is given by

$$\psi_1 = \frac{|h_{\mathrm{B1}}|^2}{d_{\mathrm{B1}}^{\alpha}} + \frac{|\mathbf{h}_{\mathrm{I1}} \times \mathbf{\Phi} \times \mathbf{h}_{\mathrm{BI}}|^2}{d_{\mathrm{BI}}^{\alpha} d_{\mathrm{I1}}^{\alpha}}. \quad (12)$$

However, in the case of a perfect CSI, we assume that all elements have the same reflection amplitude [30], [31], so $\varphi_1 = \varphi_2 = \ldots \varphi_N = \varphi$ and

$$\psi_1 = \frac{|h_{\mathrm{B1}}|^2}{d_{\mathrm{B1}}^{\alpha}} + \frac{\varphi^2}{d_{\mathrm{BI}}^{\alpha} d_{\mathrm{I1}}^{\alpha}} \left( \left| \sum_{k=1}^{N} h_{\mathrm{BI},k} h_{\mathrm{I1},k} \exp(\mathrm{j}\,\eta_k) \right| \right)^2 \quad (13)$$

where $$\eta_k = \arg(h_{\mathrm{B1},k}) - \arg(h_{\mathrm{BI},k} h_{\mathrm{I1},k}). \quad (14)$$

This leads to

$$\psi_1 = \frac{|h_{\mathrm{B1}}|^2}{d_{\mathrm{B1}}^{\alpha}} + \frac{\varphi^2}{d_{\mathrm{BI}}^{\alpha} d_{\mathrm{I1}}^{\alpha}} \left( \sum_{k=1}^{N} |h_{\mathrm{BI},k}| |h_{\mathrm{I1},k}| \right)^2 . \quad (15)$$

The signal-to-interference plus noise ratio (SINR) at User 1 when detecting signal $x_2$ is given by

$$\gamma_1^{x_2} = \frac{\rho a_2 \psi_1}{\rho a_1 \psi_1 + 1}. \quad (16)$$

At User 2, the SINR for detecting signal $x_2$ is expressed as follows

$$\gamma_2^{x_2} = \frac{\rho a_2 \psi_2}{\rho a_1 \psi_2 + 1} \quad (17)$$

where the expression of $\psi_2$ in the imperfect CSI case is given by

$$\psi_2 = \frac{|h_{\mathrm{B2}}|^2}{d_{\mathrm{B2}}^{\alpha}} + \frac{|\mathbf{h}_{\mathrm{I2}} \times \mathbf{\Phi} \times \mathbf{h}_{\mathrm{BI}}|^2}{d_{\mathrm{BI}}^{\alpha} d_{\mathrm{I2}}^{\alpha}}. \quad (18)$$

In the case of a perfect CSI, it is expressed as follows

$$\psi_2 = \frac{|h_{\mathrm{B2}}|^2}{d_{\mathrm{B2}}^{\alpha}} + \frac{\varphi^2}{d_{\mathrm{BI}}^{\alpha} d_{\mathrm{I2}}^{\alpha}} \left( \left| \sum_{k=1}^{N} h_{\mathrm{BI},k} h_{\mathrm{I2},k} \exp(\mathrm{j}\theta_k) \right| \right)^2 \quad (19)$$

with $$\theta_k = \arg(h_{\mathrm{B2}}) - \arg(h_{\mathrm{I2},k} h_{\mathrm{BI},k}). \quad (20)$$

Thus, one can obtain

$$\psi_2 = \frac{|h_{\mathrm{B2}}|^2}{d_{\mathrm{B2}}^{\alpha}} + \frac{\varphi^2}{d_{\mathrm{BI}}^{\alpha} d_{\mathrm{I2}}^{\alpha}} \left( \sum_{k=1}^{N} |h_{\mathrm{BI},k}| |h_{\mathrm{I2},k}| \right)^2 . \quad (21)$$

However, the SNR achieved by the eve to decode $x_i$ is expressed as

$$\gamma_{\mathrm{Eve}}^{x_i} = \rho_{\mathrm{Eve}} a_i \psi_{\mathrm{Eve}} \quad (22)$$

where $\psi_{\mathrm{Eve}}$ is given in the imperfect CSI case by

$$\psi_{\mathrm{Eve}} = \frac{|h_{\mathrm{BE}}|^2}{d_{\mathrm{BE}}^{\alpha}} + \frac{|\mathbf{h}_{\mathrm{IE}} \times \mathbf{\Phi} \times \mathbf{h}_{\mathrm{BI}}|^2}{d_{\mathrm{BI}}^{\alpha} d_{\mathrm{IE}}^{\alpha}} \quad (23)$$

with $$\rho_{\mathrm{Eve}} = \frac{P}{N_{\mathrm{Eve}}}. \quad (24)$$

In the case of perfect CSI, $\psi_{\mathrm{Eve}}$ is expressed by

$$\psi_{\mathrm{Eve}} = \frac{|h_{\mathrm{BE}}|^2}{d_{\mathrm{BE}}^{\alpha}} + \frac{\varphi^2}{d_{\mathrm{BI}}^{\alpha} d_{\mathrm{IE}}^{\alpha}} \left( \sum_{k=1}^{N} h_{\mathrm{IE},k} h_{\mathrm{BI},k} \exp(\mathrm{j}\delta_k) \right)^2 \quad (25)$$

where $$\delta_k = \arg(h_{\mathrm{BE},k}) - \arg(h_{\mathrm{IE},k} h_{\mathrm{BI},k}). \quad (26)$$

As consequent

$$\psi_{\mathrm{Eve}} = \frac{|h_{\mathrm{BE}}|^2}{d_{\mathrm{BE}}^{\alpha}} + \frac{\varphi^2}{d_{\mathrm{BI}}^{\alpha} d_{\mathrm{IE}}^{\alpha}} \left( \sum_{k=1}^{N} |h_{\mathrm{IE},k}| |h_{\mathrm{BI},k}| \right)^2 . \quad (27)$$

To calculate secure performance at Users 1 and 2, we define their instantaneous secrecy rates, respectively, using the following expressions

$$C_1 = \max\left\{\log_2(1+\min(\gamma_1^{x_1},\gamma_1^{x_2})) - \log_2(1+\gamma_{\text{Eve}}^{x_1}),0\right\}, \quad (28)$$

$$C_2 = \max\left\{\log_2(1+\gamma_2^{x_2}) - \log_2(1+\gamma_{\text{Eve}}^{x_2}),0\right\}. \quad (29)$$

# 3. Secrecy Performance Metrics

Though the presence of an eavesdropper in the RIS-NOMA system reduces performance for the intended users, User 1 and User 2, they remain aided by the smart reflection scheme provided by the RIS. As a result, the system continues to function effectively with the expected rates of $R_i$. However, security concerns must be verified once the situation arises in which the security rate is less than $R_i$, as the corresponding transmission cannot be guaranteed. Two key security metrics should be examined: the Secrecy Outage Probability and the Strictly Positive Secrecy Capacity, both of which are critical for evaluating security issues.

## 3.1 Secrecy Outage Probability (SOP)

The SOP can be calculated as the probability that the instantaneous secrecy capacity falls below a threshold target security rate, indicating potential vulnerabilities. It is defined by the following expression

$$\text{SOP} = \Pr\left(C_1 < R_1 \text{ or } C_2 < R_2\right). \quad (30)$$

Substituting by equations (28) and (29), the following expression can be derived [20]

$$\text{SOP} = 1 - \Pr\left(\theta_1 < th_1, \theta_2 < th_1\right)\Pr\left(\theta_3 < th_2\right) \quad (31)$$

where

$$\theta_1 = \frac{1+\gamma_1^{x_2}}{1+\gamma_{\text{Eve}}^{x_1}}, \quad (32)$$

$$\theta_2 = \frac{1+\gamma_1^{x_1}}{1+\gamma_{\text{Eve}}^{x_1}}, \quad (33)$$

$$\theta_3 = \frac{1+\gamma_2^{x_2}}{1+\gamma_{\text{Eve}}^{x_2}}, \quad (34)$$

with $th_i = 2^{R_i}$ is a threshold secure rate.

The SOP expression can be approximated in the high-SNR regime as follows [25]

$$\text{SOP} = 1 - \beta_1\left(1 - \beta_2\beta_3\exp(-\beta_4)\right)\left(1 - \exp\left(-\beta_5\right)\right) \quad (35)$$

where

$$\beta_1 = 1 - \exp\left(-\frac{a_2 - u_1 a_1}{a_1^2 th_1 \rho_{\text{Eve}} \lambda_{\phi_e}}\right), \quad (36)$$

$$\beta_2 = \frac{th_1 \rho_{\text{Eve}} \lambda_{\phi_e}}{th_1 \rho_{\text{Eve}} \lambda_{\phi_e} + \rho d_{\text{BI}}^{-\alpha}}, \quad (37)$$

$$\beta_3 = \frac{th_1 \rho_{\text{Eve}} \lambda_{\phi_e}}{th_1 \rho_{\text{Eve}} \lambda_{\phi_e} + \rho N \varphi^2 d_{\text{BI}}^{\alpha} d_{\text{II}}^{\alpha}}, \quad (38)$$

$$\beta_4 = \frac{1 - th_1}{a_1 th_1 \rho_{\text{Eve}} \lambda_{\phi_e}}, \quad (39)$$

$$\beta_5 = \frac{a_2 - a_1 u_2}{a_1 a_2 th_2 \rho_{\text{Eve}} \lambda_{\phi_e}}, \quad (40)$$

with $u_i = th_i - 1$, and $\lambda_{\phi_e} = d_{\text{BI}}^{-\alpha} + \dfrac{\varphi^2 N}{d_{\text{BI}}^{\alpha} d_{\text{IE}}^{\alpha}}$.

## 3.2 Strictly Positive Secrecy Capacity (SPSC)

The SPSC is another key performance metric for next-generation wireless technologies, including 5G, 6G, and IoT-based secure networks, emerging as a special case of the SOP when the target secrecy rates are zero. The probability of achieving a positive secrecy capacity is given by the following expression

$$\text{SPSC} = \Pr\left(th_1 < 0, th_2 < 0\right). \quad (41)$$

This metric can be expressed as follows

$$\text{SPSC} = \Pr\left(\min\left(\gamma_1^{x_2},\gamma_1^{x_1}\right) > \gamma_{\text{Eve}}^{x_1}\right)\Pr\left(\gamma_2^{x_2} > \gamma_{\text{Eve}}^{x_2}\right). \quad (42)$$

This can be approximated by the following expression

$$\text{SPSC} = \left(1 - \exp\left(-\chi_1\right)\right)\left(1 - \chi_2\chi_3\right)\left(1 - \exp\left(-\chi_4\right)\right) \quad (43)$$

where

$$\chi_1 = \frac{a_2}{a_1^2 \rho_{\text{Eve}} \lambda_{\phi_e}}, \quad (44)$$

$$\chi_2 = \frac{\rho_{\text{Eve}} \lambda_{\phi_e}}{\rho d_{\text{BI}}^{-\alpha} + \rho_{\text{Eve}} \lambda_{\phi_e}}, \quad (45)$$

$$\chi_3 = \frac{\rho_{\text{Eve}} \lambda_{\phi_e}}{\rho N \varphi^2 d_{\text{BI}}^{-\alpha} d_{\text{II}}^{-\alpha} + \rho_{\text{Eve}} \lambda_{\phi_e}}, \quad (46)$$

$$\chi_4 = \frac{1}{a_1 \rho_{\text{Eve}} \lambda_{\phi_e}}. \quad (47)$$

# 4. Optimization of Secrecy Performance Metrics

## 4.1 Problem Formulation

Improving the confidentiality of users in wireless networks, particularly when evaluating factors like the SOP and the SPSC, plays an essential role in ensuring secure communication even in the presence of potential eavesdroppers.

Fundamentally, the SOP serves as an important metric in wireless communication systems, evaluating the PLS against potential eavesdroppers. It expresses the probability that the difference between the primary and eavesdropper's channel capacities falls below a targeted secrecy rate. A heightened SOP implies an increased vulnerability to eavesdropping, whereas a reduced SOP indicates a more robustly secure transmission.

In addition, the SPSC is not just a metric; it's a fundamental concept in wireless security that guarantees a basic level of protection against eavesdropping at the physical layer. It measures the maximum rate at which private information can be transmitted from a transmitter to a receiver in the presence of eavesdroppers without the latter being able to decode any information. The SPSC ensures that a network has a non-zero secrecy rate even under challenging conditions. A high SPSC indicates that, even if an eavesdropper has better channel conditions than the legitimate receiver, there still exists a positive rate at which data can be communicated securely.

Accordingly, reducing the SOP and increasing the SPSC are crucial steps to strengthen the secrecy performance of wireless networks. To deal with this situation, we formulate the following multi-objective optimization (MOO) problem:

Find the power allocation coefficients $a_1$ and $a_2$ such that:

$$\mathrm{Min}(F_1(\mathbf{x}) = \mathrm{SOP}(\mathbf{x})) \text{ and } \mathrm{Max}(F_2(\mathbf{x}) = \mathrm{SPSC}(\mathbf{x})) \quad (48)$$

Subject to:

$$a_1 + a_2 = 1, \quad (49)$$

$$a_1 < a_2 \ . \quad (50)$$

where $\mathbf{x} = [a_1, a_2]$ is the vector of decision variables.

## 4.2 Solution Using Multi-objective AVOA

In this study, we use a multi-objective variant of the Artificial Vultures Optimization Algorithm (AVOA) called multi-objective AVOA (MOAVOA) [29] to solve the defined multi-criterion optimization problem. The concept of the AVOA was proposed by Abdollahzadeh et al. [32], inspired by the lifestyles of African vultures.

The AVOA simulates the foraging and navigation behaviors of African vultures. Based on the fundamental concepts of vultures, the algorithm is formulated in four steps [32]:

**Step 1:** Determining the best vulture in every group

Once the initial population is formed, the fitness of all solutions is evaluated. The top solution is designated as the best vulture for the first group, while the second-best solution becomes the best vulture for the second group. Other solutions, guided by (51), move towards the best solutions for both groups. In any iteration, the fitness of the entire population is recalculated.

$$\mathbf{R}(i) = \begin{cases} BestVulture_1 & \text{if } p_i = \alpha \\ BestVulture_2 & \text{if } p_i = \beta \end{cases}. \quad (51)$$

Here, $BestVulture_1$ and $BestVulture_2$ represent the first and second best vultures, respectively. $\alpha$ and $\beta$ are probability parameters between 0 and 1, and the sum of both parameters is 1. The probability of selecting the best solution is determined using the roulette wheel method for each group, as described by

$$p_i = \frac{F_i}{\sum_{i=1}^{n} F_i} \cdot \quad (52)$$

**Step 2:** Computation of the rate of starvation of vultures

At this phase, the vultures' hunger level is calculated, and this behavior is mathematically represented by the following expression

$$F = \left(2 \cdot rand_1 + 1\right) \cdot y \cdot \left(1 - \frac{iteration_i}{Max\,iterations}\right) \quad (53)$$

where $F$ is the amount of hunger, $y$ random number between –1 and 1, and $rand_1$ is a random number between 0 and 1. When $|F|$ exceeds 1, the AVOA algorithm transitions into the exploration phase. Conversely, when $|F|$ is less than 1, the algorithm shifts into the exploitation phase, where vultures focus on searching for food in their immediate vicinity.

**Step 3:** Exploration

During the exploration stage, the movement of the vultures is defined by the following equations

$$\mathbf{V}(i+1) = \mathbf{R}(i) - \mathbf{D}(i) \cdot F \quad \text{if } p_1 \geq rand_{p1} \quad (54)$$

where

$$\mathbf{D}(i) = \left| X \cdot \mathbf{R}(i) - \mathbf{V}(i) \right|, \quad (55)$$

and

$$\mathbf{V}(i+1) = \mathbf{R}(i) - F + rand_2((ub - lb) \cdot rand_3 + lb) \quad \text{if } p_1 < rand_{p1} \quad (56)$$

where $\mathbf{V}(i+1)$ is the vulture's position vector in the next iteration. $F$ denotes the satisfaction level of the vulture, as defined by (53), $\mathbf{R}(i)$ is calculated using (51), while $X$ represents the stochastic movement of the vulture leader. This random movement is determined by $X = 2\times rand$, where $rand$ is a randomly generated number between 0 and 1. The current position vector of the vultures is given by $\mathbf{V}(i)$. Additionally, $rand_2$ and $rand_3$ are also random values within the [0, 1] interval. Finally, $ub$ and $lb$ represent the upper and lower bounds of the variables, respectively.

**Step 4:** Exploitation

This stage consists of two phases, each employing distinct strategies. The selection of a strategy in each phase is governed by two parameters, $p_2$ and $p_3$. Parameter $p_2$ dictates the choice of strategies in the first phase, while $p_3$ controls the strategy selection in the second phase. Both parameters must be assigned values within the range [0, 1] prior to initiating the search operation. The first exploitation phase is performed when $|F| \geq 0.5$, and the vultures' movement during this phase is described by the following equations

$$\mathbf{V}(i+1) = \mathbf{D}(i) \cdot (F + rand_4) - d(t) \quad \text{if } p_2 \geq rand_{p2} \tag{57}$$

where

$$d(t) = \mathbf{R}(i) - \mathbf{V}(i), \tag{58}$$

and

$$\begin{aligned}&\mathbf{V}(i+1) = \\ &\mathbf{D}(i) \cdot \exp(SF) \cdot \cos(2\pi F) + \mathbf{R}(i) \quad \text{if } p_2 < rand_{p2}\end{aligned} \tag{59}$$

where $\mathbf{V}(i+1)$ is the vulture's position vector in the next iteration. The variable $rand_4$ represents a randomly generated number between 0 and 1. In (58), $\mathbf{R}(i)$ is obtained through (51), and $\mathbf{V}(i)$ represents the position vector, which is used to determine the distance between a given vulture and one of the top-performing individuals. In (59), the parameter $S$ defines the spiral form of the logarithm model.

In the second phase of exploitation, when $|F| < 0.5$, this phase is performed and the vultures' movement is governed by the following equations

$$\mathbf{V}(i+1) = \frac{A_1 + A_2}{2} \text{ if } p_3 \geq rand_{p3} \tag{60}$$

where

$$\begin{aligned}A_1 &= \mathbf{BestV}_1(i) - \mathbf{D}(i) \cdot F, \\ A_2 &= \mathbf{BestV}_2(i) - \mathbf{D}(i) \cdot F\end{aligned} \tag{61}$$

and

$$\mathbf{V}(i+1) = \mathbf{R}(i) - |d(t)| \cdot F \cdot \text{Levy}(d) \quad \text{if } p_3 < rand_{p3} \tag{62}$$

where the $\mathbf{BestV}_1(i)$ denotes the best-performing vulture in the first group, while $\mathbf{BestV}_2(i)$ represents the best vulture in the second group. In (62), the Levy flight (LF) is computed by

$$\begin{aligned}&\text{LF}(x) = 0.01 \frac{u \cdot \sigma}{|v|^{1/\beta}}, \\ &\sigma = \left( \frac{\Gamma(1+\beta) \cdot \sin\left(\frac{\pi\beta}{2}\right)}{\Gamma\left((1+\beta)/2\right) \cdot \beta \cdot 2^{\left(\frac{\beta-1}{2}\right)}} \right)^{1/\beta}\end{aligned} \tag{63}$$

where $u$ and $v$ are random numbers between 0 and 1, and $\beta$ is fixed to 1.5.

The AVOA has three new mechanisms for performing multi-objective optimization, similar to those employed by Multi-objective Grey Wolf Optimizer: an archive, a grid mechanism and a leader selection mechanism [29], [33]. The pseudo code MOAVOA applied to our two-objective trade-off problem is explained in Algorithm 1.

---

**Problem definition**: Define Vector of decision variables $\mathbf{x} = [a_1, a_2]$ and working space boundaries of decision variables.
MOAVOA parameters: Maximum number of iterations (*Maxit*), Population size (*nPop*), Grid Inflation Parameter (*α*), Number of Grids per each Dimension (*nGrid*), Leader Selection Pressure Parameter (*β*), Extra Repository Member Selection Pressure (*γ*).
**Initialize (*Pop*):** Initialize the random population $xi$ ($i$ = 1, 2,…, *nPop*) with random combinations of [$a_1$, $a_2$]
**Evaluate (*Pop*):** Calculate the objective values of all population.
**Obtain** the non-dominated solutions and create the archive.
**Find** the leader
**While** *(stopping condition is not met)* **do**
  **Calculate** the fitness values of Vulture
  **Set** $x_{\text{Vulture}}$ as the location of Vulture (1st best location Best Vulture Category 1)
  **Set** $x_{\text{Vulture}}$ as the location of Vulture (2nd best location Best Vulture Category 2)
  **For** ($i$ = 1 to *nPop*) **do**
    **Update** the $F$ using (53)
    **Select** $\mathbf{R}(i)$ using (51 and 52)
    **If** ( $|F| \geq 1$ ) **then**
      **If** ( $p_1 \geq rand_{p_1}$ ) **then**
        **Update** the location of Vulture by (54)
      **else**
        **Update** the location of Vulture by (56)
    **If** ( $|F| < 1$ ) **then**
      **If** ( $|F| \geq 0.5$ ) **then**
        **If** ( $p_2 \geq rand_{p_2}$ ) **then**
          **Update** the location of Vulture by (57)
        **else**
          **Update** the location Vulture by (59)
      **else If** ( $|F| < 0.5$ ) **then**
        **If** ( $p_3 \geq rand_{p_3}$ ) **then**
          **Update** the location Vulture by (60)
        **else**
          **Update** the location Vulture by (62)
  **Evaluate** the objective values for all population
  **Obtain** the non-dominated solution
  **Update** the Archive according to the found non-dominated solutions
    **If** (Archive = full) **then**
      **Use** the grid mechanism to delete the current archives
      **Add** the new solution to the Archive
    **If** (any of the newly added answers to the Archive is placed outside of the hypercubes) **then**
      **Update** the grids
**Return** the Archive

---

**Algorithm 1.** Pseudo code of MOAVOA algorithm [29].

## 5. Simulation and Results Discussion

To evaluate the effectiveness of the proposed algorithm, this section presents simulation results. As previously outlined, the objective of the MOAVOA algorithm is to identify the optimal values for the power allocation coefficients $a_1$ and $a_2$ while adhering to the constraints defined in (49) and (50), such that $\mathrm{Min}(F_1(\mathbf{x}) = \mathrm{SOP}(\mathbf{x}))$ and $\mathrm{Max}(F_2(\mathbf{x})=\mathrm{SPSC}(\mathbf{x}))$.

This issue is reframed as

$$\mathrm{Min}(f_1, f_2) \tag{64}$$

where $f_1$ and $f_2$ indicate the fitness functions given by

$$f_1 = \sum_{\rho=-25}^{30} F_1(\mathbf{x}) = \sum_{\rho=-25}^{30} \mathrm{SOP}(\mathbf{x}), \tag{65}$$

$$f_2 = \frac{100}{\sum_{\rho=-25}^{30} F_2(\mathbf{x})} = \frac{100}{\sum_{\rho=-25}^{30} \mathrm{SPSC}(\mathbf{x})}. \tag{66}$$

The effectiveness of the proposed MOAVOA method is evaluated by comparing its results with those of Multi-objective Particle Swarm Optimization (MOPSO) algorithm. Both algorithms were studied using important system parameters presented in Tab. 1 [25] and the control parameters listed in Tab. 2 and 3.

In this system model, the eavesdropper is an illegitimate user located near the NOMA users, intercepting the signal reflected from the RIS, which originates from the BS. The received signal is affected by additive white Gaussian noise (AWGN) and is dependent on the following parameters: small-scale fading between the BS and the RIS, small-scale fading between the RIS and the eavesdropper, distance between the BS and the RIS, distance between the RIS and the eavesdropper, amplitude reflection coefficients of the RIS elements and phase shift variables introduced by the reflective elements of the RIS. In the simulation, these parameters are randomly generated under both perfect and imperfect CSI conditions as follows:

| Parameter | Value |
|---|---|
| SNR ratio $\rho$ (dB) | [–25, 30] |
| Number of reflecting elements of the RIS($N$) | 50 |
| Power allocation coefficients ($a_1$, $a_2$) | [0, 1] |
| Target rates ($R_1$, $R_2$) (bps/Hz) | 0.1 |
| Path loss exponent ($\alpha$) | 4 |
| Distances ($d_{\mathrm{B1}}$, $d_{\mathrm{B2}}$, $d_{\mathrm{BE}}$) (Normalized) | 0.8 |
| Distances ($d_{\mathrm{BI}}$, $d_{\mathrm{I1}}$, $d_{\mathrm{I2}}$) (Normalized) | 1 |
| Distance ($d_{\mathrm{IE}}$) (Normalized) | 0.7 |
| SNR ratio $\rho_{\mathrm{Eve}}$ (dB) | 19 |

**Tab. 1.** The system parameters.

| Parameter | Value |
|---|---|
| Population size (*nPop*) | 100 |
| Maximum number of iterations (*Maxit*) | 100 |
| Inertia Weight (*w*) | 0.4 |
| Personal Learning Coefficient ($c_1$) | 1 |
| Global Learning Coefficient ($c_2$) | 2 |
| Leader selection pressure (β) | 2 |
| Mutation Rate (*Mu*) | 0.1 |
| Number of grids per dimension (*nGrid*) | 7 |
| Maximum number of repository (*nRep*) | 100 |

**Tab. 2.** MOPSO parameters.

| Parameter | Value |
|---|---|
| Population size (*nPop*) | 100 |
| Maximum number of iterations (*Maxit*) | 100 |
| Archive size (*Asize*) | 100 |
| Grid Inflation Parameter ($\alpha$) | 0.1 |
| Number of grids (*nGrid*) | 10 |
| Leader selection pressure ($\beta$) | 4 |
| Extra Repository Member Selection Pressure ($\gamma$) | 2 |

**Tab. 3.** MOAVOA parameters.

- Imperfect CSI:

- Amplitude reflection coefficients vary between 0 and 1.
- Phase shifts vary between 0 and 2π.

- Perfect CSI:

- All RIS elements have identical reflection amplitudes and uniform phase shifts.

Furthermore, the Rayleigh fading channel parameters used in the simulation are as follows:
- Distances (Direct Links): BS to RIS, BS to User 1, BS to User 2, and BS to Eavesdropper.
- Distances (Indirect Links via RIS): RIS to User 1, RIS to User 2 and RIS to Eavesdropper
- Path Loss Exponent: $\alpha = 4$ for the Rayleigh fading channel
- Small-Scale Fading (Direct Links): BS to RIS, BS to User 1, BS to User 2, and BS to Eavesdropper.
- Small-Scale Fading (Indirect Links via RIS): RIS to User 1, RIS to User 2, and RIS to Eavesdropper.
- Additional RIS Parameters:
  - Amplitude reflection coefficients,
  - Phase shift variables.

In the simulation, these parameters are assigned random values for both perfect and imperfect CSI scenarios, as discussed in the previous section.

Additionally, according to the literature, the number of RIS elements $N$ typically ranges from tens to hundreds, depending on the specific use case (e.g., indoor vs. outdoor environments, small-scale vs. large-scale deployments). In this study, $N = 50$ is selected as an optimal trade-off between performance and computational complexity, ensuring a meaningful system evaluation.

The optimal solutions obtained by both MOPSO and MOAVOA methods are as indicated in Tab. 4 and Tab. 5, corresponding to perfect and imperfect CSI cases, respectively.

Figures 2 and 3 illustrate the optimal extracted solutions using the MOPSO and MOAVOA algorithms, demonstrating a good trade-off between both objectives for the perfect and imperfect CSI cases, respectively. The results clearly indicate that the MOAVOA algorithm outperforms the MOPSO method in terms of optimization efficiency. Thus, the MOAVOA presents high convergence and coverage within just 10 iterations, requiring only 2.119346 seconds to converge to the optimal solution.

Figures 4 and 5 represent the SOP metric versus SNR for both perfect and imperfect CSI cases, evaluated across

| | $f_1$ | $f_2$ | $a_1$ | $a_2$ |
|---|---|---|---|---|
| **Best solution ($X_1$) using MOPSO** | 11.4288 | 7.9046 | 0.1031 | 0.8969 |
| **Best solution ($X_2$) using MOAVOA** | 11.2856 | 7.8038 | 0.1000 | 0.9000 |

**Tab. 4.** Simulation results of MOPSO and MOAVOA for perfect CSI case for $N = 50$.

| | $f_1$ | $f_2$ | $a_1$ | $a_2$ |
|---|---|---|---|---|
| **Best solution ($X_1$) using MOPSO** | 12.0242 | 8.3469 | 0.1029 | 0.8971 |
| **Best solution ($X_2$) using MOAVOA** | 11.8826 | 8.2379 | 0.1000 | 0.9000 |

**Tab. 5.** Simulation results of MOPSO and MOAVOA for imperfect CSI case for $N = 50$.

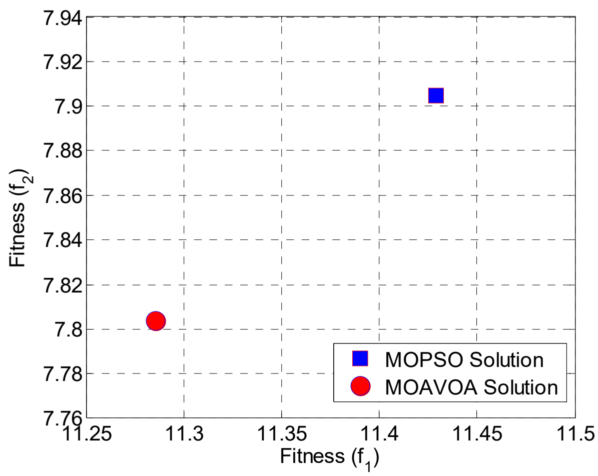


**Fig. 2.** MOPSO and MOAVOA solutions for perfect CSI case ($N = 50$).

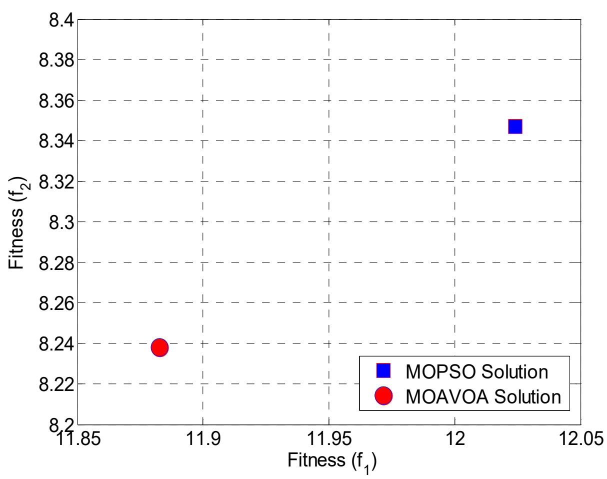


**Fig. 3.** MOPSO and MOAVOA solutions for imperfect CSI case ($N = 50$).

various power allocation coefficients with $N = 50$. The results demonstrate that lower outage probability levels are achieved for lower values of the power allocation coefficient of the nearby user from the BS, consistent with the optimal solution provided by the MOAVOA algorithm. A lower SOP indicates that the legitimate channel consistently outperforms the eavesdropper's channel, reflecting robust security and efficient resource allocation.

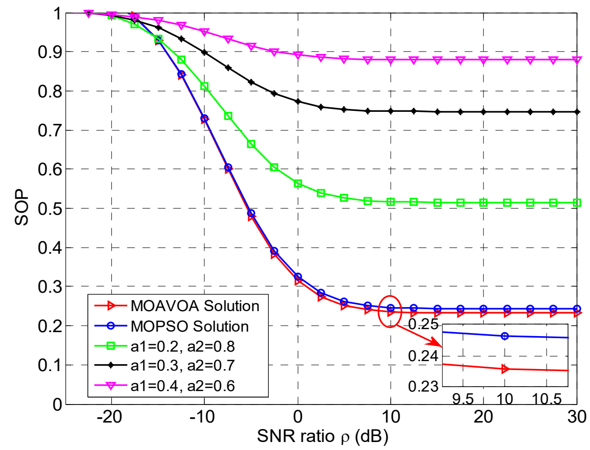


**Fig. 4.** SOP performance versus SNR ratio for $N = 50$ (Perfect CSI case),

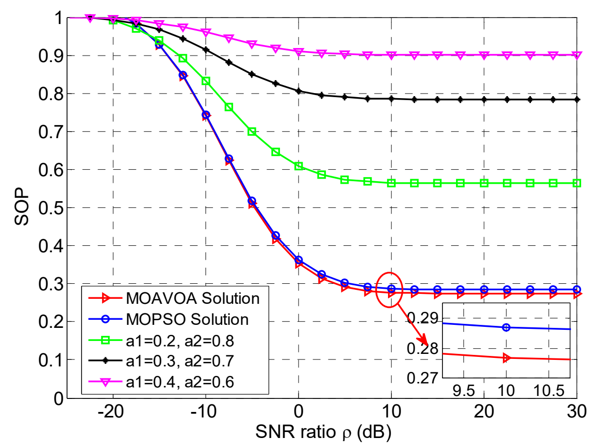


**Fig. 5.** SOP performance versus SNR ratio for $N = 50$ (Imperfect CSI case),

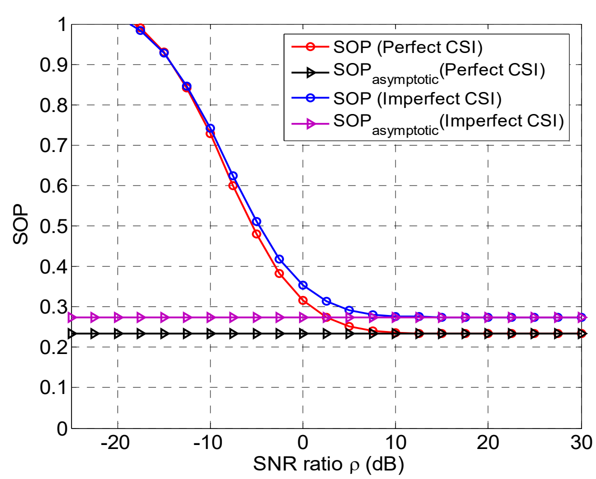


**Fig. 6.** SOP and asymptotic SOP for perfect and imperfect CSI using $N = 50$ and MOAVOA solution.

Figure 6 presents the SOP metric along with its asymptotic values for both perfect and imperfect CSI cases, using $N = 50$ and power allocation coefficients obtained through the MOAVOA algorithm. One can observe that the perfect CSI case performs a lower outage probability compared to the imperfect CSI case.

The key reason for this lower SOP in the perfect CSI case is the accuracy and certainty in channel knowledge, which enables precise power allocation, ensuring that the legitimate user's channel consistently outperforms the eavesdropper’s. In contrast, imperfect CSI introduces uncertainties, slightly complicating the achievement of optimal performance and marginally increasing the probability of secrecy outages.

Figures 7 and 8 illustrate the SPSC metric as a function of SNR for both perfect and imperfect CSI scenarios, evaluated under different power allocation coefficients, with $N = 50$. The results show that higher SPSC levels are obtained with lower power allocation coefficients for the nearby user relative to the BS, aligning with the optimal solution identified by the MOAVOA algorithm. A higher SPSC indicates that:

- The RIS-aided NOMA network can support more secure connections, allowing for larger-scale deployments in IoT, V2X (Vehicle-to-Everything), and smart grid communications.
- Secure communication can be maintained over a broader range of SNR values, enhancing system robustness in varying channel conditions. This is particularly useful in 5G and beyond networks, where security threats are more sophisticated.
- The legitimate user consistently has a significant advantage over the eavesdropper, making it difficult for the latter to intercept or decode the signal. This is beneficial for military and financial applications, where data security is paramount.
- Even if channel conditions degrade slightly, secure communication can still be maintained without frequent interruptions or the need for additional encryption mechanisms.

Figure 9 illustrates the SPSC metrics alongside their asymptotic values for both perfect and imperfect CSI scenarios, using $N = 50$ and power allocation coefficients determined by the MOAVOA algorithm. It is evident that the perfect CSI case achieves a higher SPSC compared to the imperfect case. The performance gap between perfect and imperfect CSI in terms of SPSC is primarily due to the accuracy and reliability of channel knowledge, which directly influences power and resource allocation as well as signal transmission strategies.

Figures 10 and 11 represent the SOP metric as a function of SNR for both perfect and imperfect CSI scenarios, evaluated under different values of target rates $R_1$, $R_2$ assigned to the users. The results show that better SOP per-

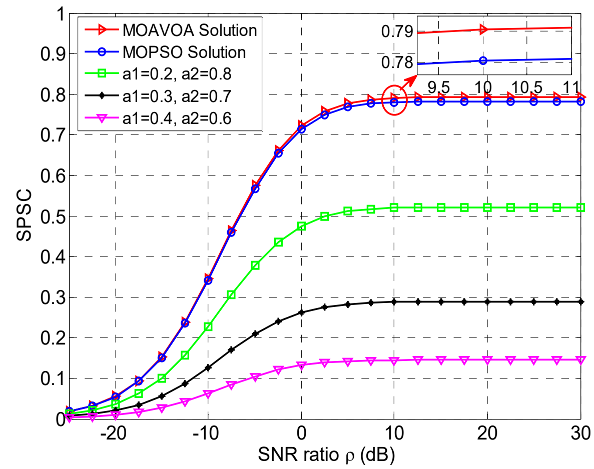


**Fig. 7.** SPSC performance versus SNR ratio for $N = 50$ (Perfect CSI case).

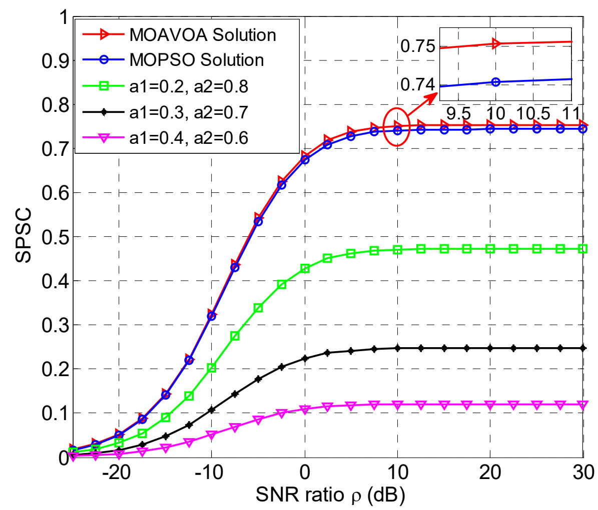


**Fig. 8.** SPSC performance versus SNR ratio for $N = 50$ (Imperfect CSI case).

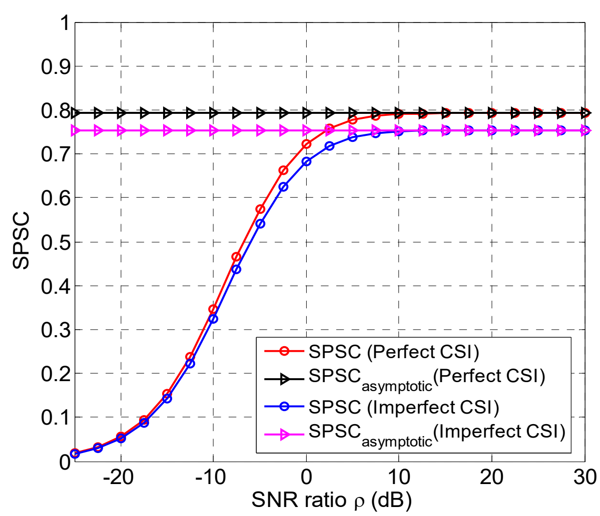


**Fig. 9.** SPSC and asymptotic SPSC for perfect and imperfect CSI using $N = 50$ and MOAVOA solution.

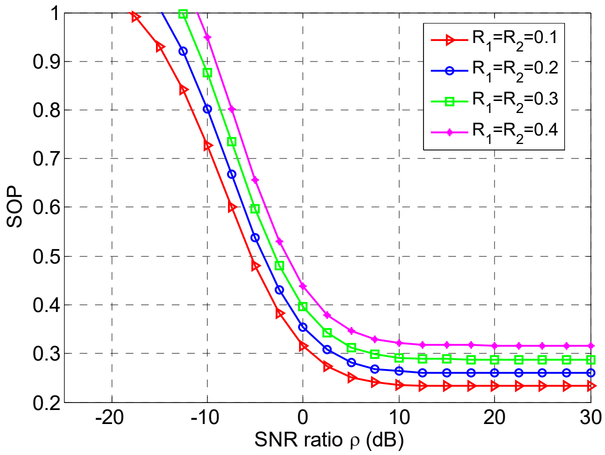


**Fig. 10.** SOP performance versus SNR ratio for different $R_1 = R_2$ and $N = 50$ (Perfect CSI case).

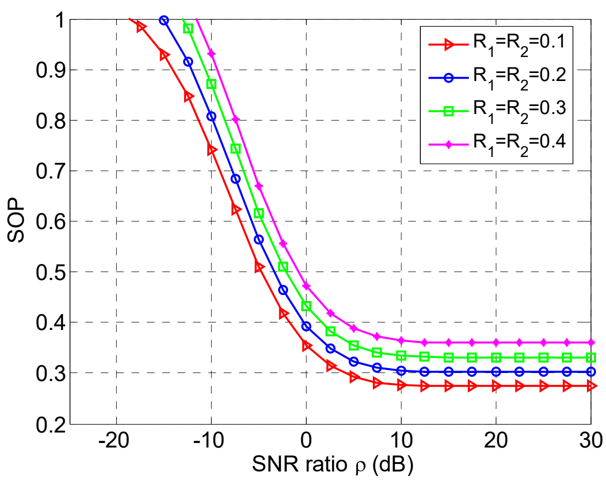


**Fig. 11.** SOP performance versus SNR ratio for different $R_1 = R_2$ and $N = 50$ (Imperfect CSI case).

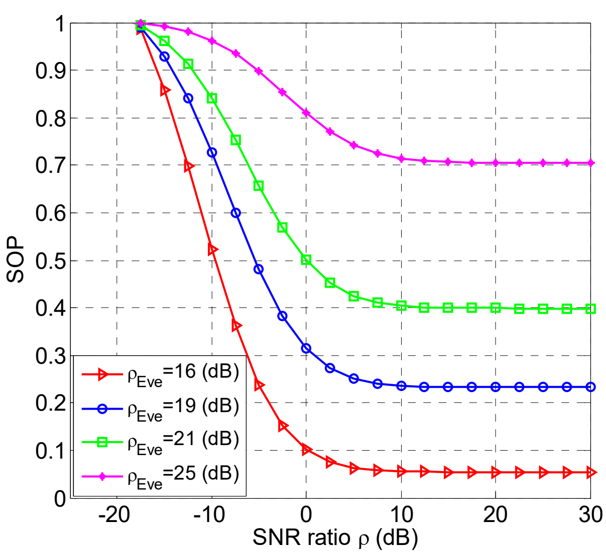


**Fig. 12.** SOP performance versus SNR ratio for different $\rho_{\mathrm{Eve}}$ and $N$=50 (Perfect CSI case).

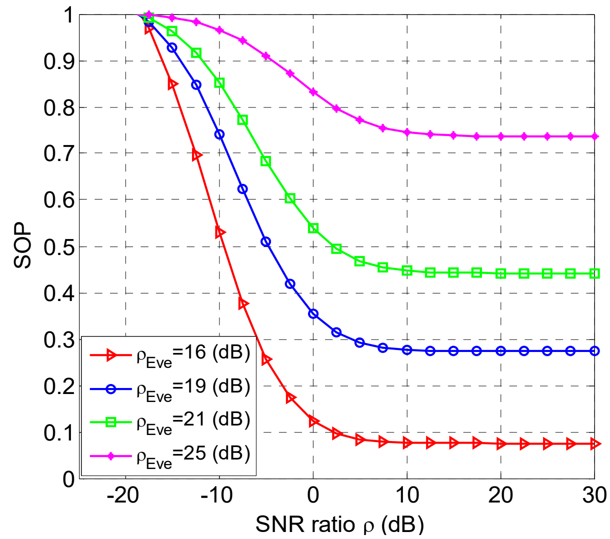


**Fig. 13.** SOP performance versus SNR ratio for different $\rho_{\mathrm{Eve}}$ and $N = 50$ (Imperfect CSI case).

formance is obtained with lower values of $R_1$ and $R_2$. Thus, higher target rates increase SOP, leading to greater eavesdropping risks.

A similar SOP trend is observed when $\rho_{\mathrm{Eve}}$ increases, as illustrated in Fig. 12 and 13. Thus, higher $\rho_{\mathrm{Eve}}$ reduces the secrecy capacity of legitimate users, increasing the probability that the secrecy rate falls below the required threshold, thereby raising SOP.

Figures 14 and 15 illustrate the SPSC performance for both perfect and imperfect CSI cases, evaluated under different values of $\rho_{\mathrm{Eve}}$. We can see that as $\rho_{\mathrm{Eve}}$ increases, the eavesdropper can decode more information, thereby reducing secrecy capacity values.

Figures 16, 17, 18 and 19 show the impact of varying the number of RIS elements on SOP and SPSC performance for both perfect and imperfect CSI scenarios. The results clearly demonstrate that increasing the number of RIS elements significantly improves secrecy performance, reducing SOP and enhancing SPSC efficiency. We notice that saturation point happens at $\rho = 10$ dB.

## 6. Conclusion

This paper analyzes the PLS of RIS-aided downlink NOMA networks in the presence of eavesdropping threats. In this system, paired users communicate simultaneously with the BS and the RIS. By analyzing reflected links under Rayleigh fading, we derive new channel statistics and evaluate the network's performance using two key security metrics: SOP and SPSC. The analysis is conducted for both perfect and imperfect CSI scenarios. To optimize SOP and SPSC, we employ the multi-objective artificial vulture's optimization algorithm, focusing on the power allocation coefficients for nearby and distant users. The results highlight that a reduced power allocation coefficient for the

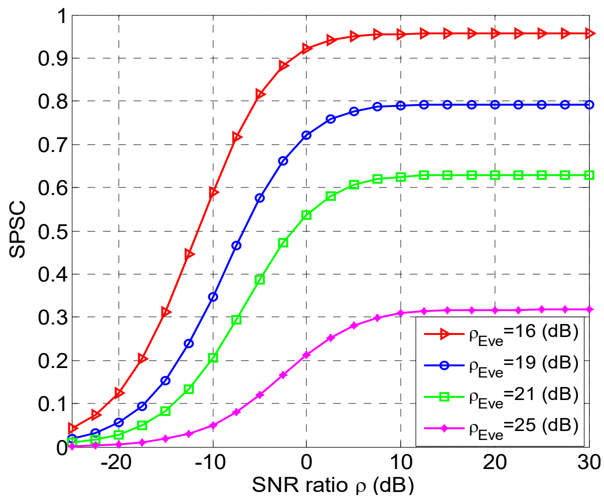


**Fig. 14.** SPSC performance versus SNR ratio for different $\rho_{Eve}$ and $N = 50$ (Perfect CSI case).

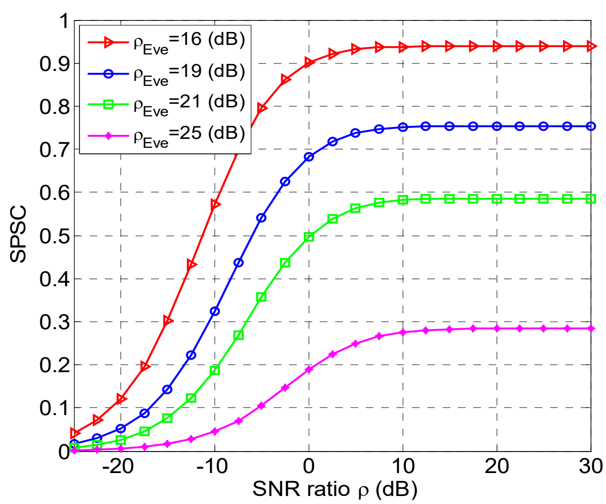


**Fig. 15.** SPSC performance versus SNR ratio for different $\rho_{Eve}$ and $N = 50$ (Imperfect CSI case).

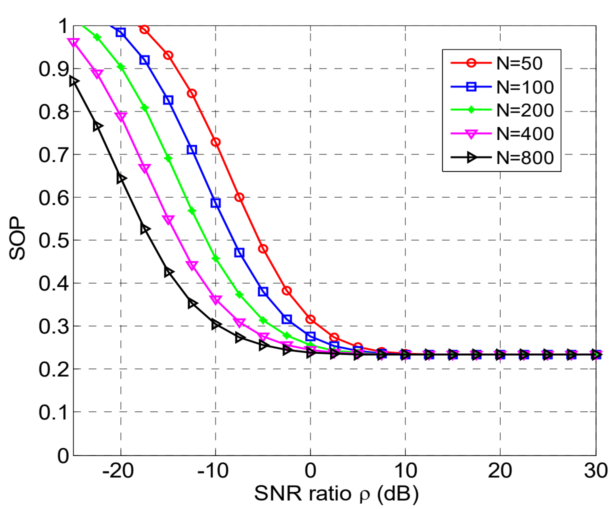


**Fig. 16.** SOP performance versus SNR ratio for different $N$ (Perfect CSI case).

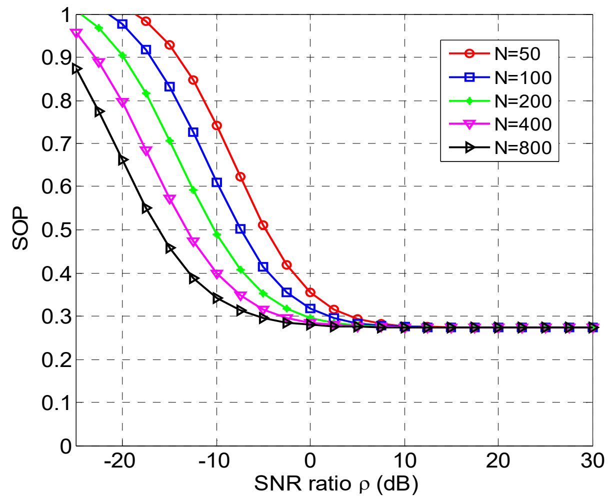


**Fig. 17.** SOP performance versus SNR ratio for different $N$ (Imperfect CSI case).

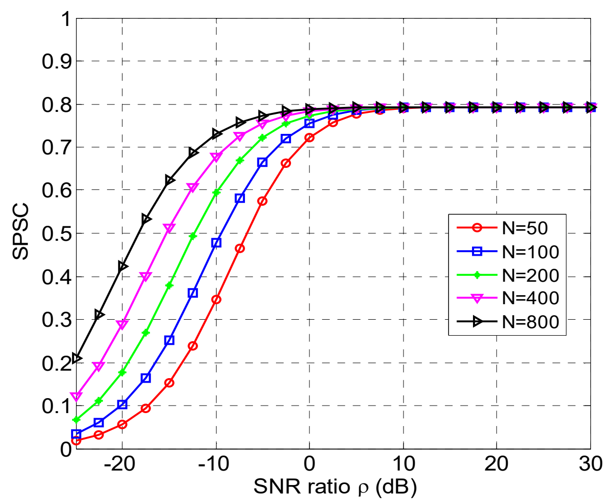


**Fig. 18.** SPSC performance versus SNR ratio for different $N$ (Perfect CSI case).

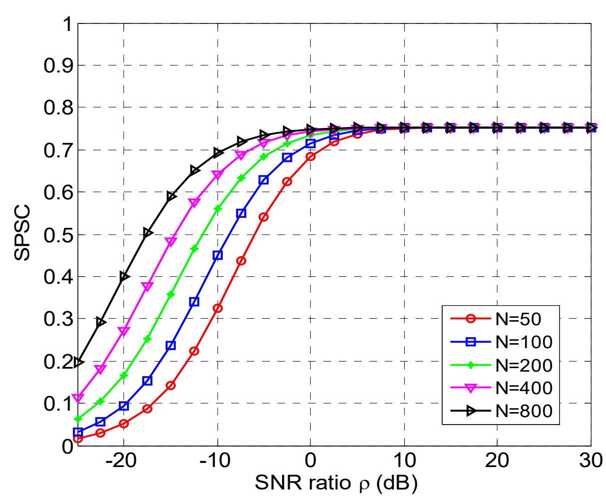


**Fig. 19.** SPSC performance versus SNR ratio for different $N$ (Imperfect CSI case).

nearby user leads to lower SOP values and higher SPSC levels, reflecting the effectiveness of MOAVOA in identifying optimal solutions. Moreover, the findings reveal that perfect CSI slightly enhances security performance, with lower SOP and higher SPSC compared to the imperfect CSI scenario. This demonstrates the critical role of accurate channel estimation in maintaining robust PLS. This study confirms the significant benefit of integrating RIS and NOMA in enhancing the performance of wireless communication under attack from eavesdroppers. Thus, it can be extended to emerging technologies to investigate secrecy performance in 6G networks and beyond such as terahertz and visible light communication (VLC) systems. It can also be employed for UAV-assisted secure networks, where secrecy optimization for drone-based communication systems in military and civilian applications is highly requested. Additionally, a hybrid approach that integrates advanced machine learning techniques such as Deep Neural Networks (DNN) and multi-objective optimization algorithms can be considered for adaptive optimization to achieve a real-time secure transmission in RIS-aided NOMA networks under dynamic eavesdropping threats, where the eavesdropper's position continuously changes.

## Acknowledgments

This work is partially supported by the UK Engineering and Physical Sciences Research Council (EPSRC) under grant EP/Y035135/1, and HORIZON-MSCA-2022-SE-01-01-ID: 101131501, Marie Skłodowska-Curie, Research and Innovation Staff Exchange (RISE), titled: 6G Terahertz Communications for Future Heterogeneous Wireless Network (6G-TERAFIT).

## References

[1] DING, Z., YANG, Z., FAN, P., et al. On the performance of non-orthogonal multiple access in 5G systems with randomly deployed users. *IEEE signal processing letters*, 2014, vol. 21, no. 12, p. 1501–1505. DOI: 10.1109/LSP.2014.2343971

[2] ZENG, M., YADAV, A., DOBRE, O. A., et al. Energy-efficient joint user-RB association and power allocation for uplink hybrid NOMA-OMA. *IEEE Internet of Things Journal*, 2019, vol. 6, no. 3, p. 5119–5131. DOI: 10.1109/JIOT.2019.2896946

[3] HASHEMI, R., BEYRANVAND, H., MILI, M. R., et al. Energy efficiency maximization in the uplink delta-OMA networks. *IEEE Transactions on Vehicular Technology*, 2021, vol. 70, no. 9, p. 9566–9571. DOI: 10.1109/TVT.2021.3097128

[4] LIU, Y., ZHANG, S., MU, X., et al. Evolution of NOMA toward next generation multiple access (NGMA) for 6G. *IEEE Journal on Selected Areas in Communications*, 2022, vol. 40, no. 4, p. 1037–1071. DOI: 10.1109/JSAC.2022.3145234

[5] DING, Z., POOR, H. V. A simple design of IRS-NOMA transmission. *IEEE Communications Letters*, 2020, vol. 24, no. 5, p. 1119–1123. DOI: 10.1109/LCOMM.2020.2974196

[6] HUANG, C., ZAPPONE, A., ALEXANDROPOULOS, G. C., et al. Reconfigurable intelligent surfaces for energy efficiency in wireless communication. *IEEE Transactions on Wireless Communications*, 2019, vol. 18, no. 8, p. 4157–4170. DOI: 10.1109/TWC.2019.2922609

[7] NI, Y., LIU, Y., WANG, J., et al. Performance analysis for RIS-assisted D2D communication under Nakagami-m fading. *IEEE Transactions on Vehicular Technology*, 2021, vol. 70, no. 6, p. 5865–5879. DOI: 10.1109/TVT.2021.3077805

[8] ZUO, J., LIU, Y., BASAR, E., et al. Intelligent reflecting surfaces enhanced millimeter-wave NOMA systems. *IEEE Communications Letters*, 2020, vol. 24, no. 11, p. 2632–2636. DOI: 10.1109/LCOMM.2020.3009158

[9] YANG, L., YANG, J., XIE, W., et al. Secrecy performance analysis of RIS-aided wireless communication systems. *IEEE Transactions on Vehicular Technology*, 2020, vol. 69, no. 10, p. 12296–12300. DOI: 10.1109/TVT.2020.3007521

[10] YANG, L., YUAN, Y. Secrecy outage probability analysis for RIS-assisted NOMA systems. *Electronics Letters*, 2020, vol. 56, no. 23, p. 1254–1256. DOI: 10.1049/el.2020.2284

[11] LIAN, X., YUE, X., LI, X., et al. Reconfigurable intelligent surface assisted non-terrestrial NOMA networks. *Wireless Communications and Mobile Computing*, 2022, vol. 2022, p. 1–13. DOI: 10.1155/2022/8494630

[12] GONG, S., LU, X., HOANG, D. T., et al. Toward smart wireless communications via intelligent reflecting surfaces: A contemporary survey. *IEEE Communications Surveys & Tutorials*, 2020, vol. 22, no. 4, p. 2283–2314. DOI: 10.1109/COMST.2020.3004197

[13] LIU, Y., OUYANG, C., DING, Z., et al. The road to next-generation multiple access: A 50-year tutorial review. *Proceedings of the IEEE*, 2024, vol. 112, no. 9, p. 1100–1148. DOI: 10.1109/JPROC.2024.3476675

[14] ZHANG, C., YI, W., LIU, Y., et al. Downlink analysis for reconfigurable intelligent surfaces aided NOMA networks. In *IEEE Global Communications Conference (GLOBECOM)*. Taipei (Taiwan), 2020, p. 1–6. DOI: 10.1109/GLOBECOM42002.2020.9322367

[15] CHEN, S., SUN, S., KANG, S. System integration of terrestrial mobile communication and satellite communication — the trends, challenges and key technologies in B5G and 6G. *China Communications*, 2020, vol. 17, no. 12, p. 156–171. DOI: 10.23919/JCC.2020.12.011

[16] GE, R., BIAN, D., CHENG, J., et al. Joint user pairing and power allocation for NOMA-based GEO and LEO satellite network. *IEEE Access*, 2021, vol. 9, p. 93255–93266. DOI: 10.1109/ACCESS.2021.3078458

[17] HAN, L., ZHU, W. P., LIN, M. Outage of NOMA-based hybrid satellite-terrestrial multi-antenna DF relay networks. *IEEE Wireless Communications Letters,* 2021, vol. 10, no. 5, p. 1083–1087. DOI: 10.1109/LWC.2021.3058005

[18] ARANITI, G., IERA, A., PIZZI, S., et al. Toward 6G non-terrestrial networks. *IEEE Network,* 2022, vol. 36, no. 1, p. 113–120. DOI: 10.1109/MNET.011.2100191

[19] GUAN, D., SUN, X., WANG, J., et al. RIS-NOMA-aided LEO satellite communication networks. In *10th International Conference on Information Systems and Computing Technology (ISCTech)*. Guilin (China), 2022, p. 409–413. DOI: 10.1109/ISCTech58360.2022.00071

[20] LIU, Y., MU, X., LIU, X., et al. Reconfigurable intelligent surface-aided multi-user networks: interplay between NOMA and RIS. *IEEE Wireless Communications*, 2022, vol. 29, no. 2, p. 169–176. DOI: 10.1109/MWC.102.2100363

[21] ALMOHAMAD, A., AL-KABABJI, A., TAHIR, A., et al. On optimizing the secrecy performance of RIS-assisted cooperative networks. In *IEEE 92nd Vehicular Technology Conference (VTC2020-Fall)*. Victoria (BC, Canada), 2020, p. 1–5. DOI: 10.1109/VTC2020-Fall49728.2020.9348668

[22] TRIGUI, I., AJIB, W., ZHU, W. Secrecy outage probability and average rate of RIS-aided communications using quantized phases. *IEEE Communications Letters*, 2021, vol. 25, no. 6, p. 1820–1824. DOI: 10.1109/LCOMM.2021.3057850

[23] ZHANG, Z., ZHANG, C., JIANG, C., et al. Improving physical layer security for reconfigurable intelligent surface aided NOMA 6G networks. *IEEE Transactions on Vehicular Technology*, 2021, vol. 70, no. 5, p. 4451–4463. DOI: 10.1109/TVT.2021.3068774

[24] TANG, Z., HOU, T., LIU, Y., et al. Physical layer security of intelligent reflective surface aided NOMA networks. *IEEE Transactions on Vehicular Technology*, 2022, vol. 71, no. 7, p. 7821–7834. DOI: 10.1109/TVT.2022.3168392

[25] DANG, H. P., VAN NGUYEN, M. S., DO, D. T., et al. Secure performance analysis of aerial RIS-NOMA-aided systems: Deep neural network approach. *Electronics*, 2022, vol. 11, no. 16, p. 1–19. DOI: 10.3390/electronics11162588

[26] TITEL, F., BELATTAR, M. Security performance optimization of aerial downlink NOMA-IRS aided networks. In *International Conference on Electrical Engineering and Advanced Technology (ICEEAT)*. Batna (Algeria), 2023, p. 1–6. DOI: 10.1109/ICEEAT60471.2023.10426005

[27] BEIGIAN, A., KIANFAR, G., ABOUEI, J., et al. Enhancing security for physical layer communication in RIS-aided MIMO-NOMA systems in the presence of an eavesdropper. *Physical Communication*, 2024, vol. 64, p. 1–17. DOI: 10.1016/j.phycom.2024.102333

[28] LE, T. L., NGUYEN, B. C., HOANG, T. M., et al. Improving secrecy performance of NOMA networks with multiple non-colluding eavesdroppers employing multiple aerial reconfigurable intelligent surfaces. *Physical Communication*, 2024, vol. 63, p. 1–15. DOI: 10.1016/j.phycom.2024.102314

[29] KHODADADI, N., SOLEIMANIAN GHAREHCHOPOGH, F., MIRJALILI, S. MOAVOA: A new multi-objective artificial vultures optimization algorithm. *Neural Computing and Applications,* 2022, vol. 34, no. 23, p. 20791–20829. DOI: 10.1007/s00521-022-07557-y

[30] WU, C., YAN, S., ZHOU, X., et al. Intelligent reflecting surface (IRS)-aided covert communication with warden's statistical CSI. *IEEE Wireless Communications Letters,* 2021, vol. 10, no. 7, p. 1449–1453. DOI: 10.1109/LWC.2021.3069778

[31] ZHAO, W., WANG, G., ATAPATTU, S., et al. Is backscatter link stronger than direct link in reconfigurable intelligent surface-assisted system? *IEEE Communications Letters,* 2020, vol. 24, no. 6, p. 1342–1346. DOI: 10.1109/LCOMM.2020.2980510

[32] ABDOLLAHZADEH, B., GHAREHCHOPOGH, F. S., MIRJALILI, S. African vultures optimization algorithm: A new nature-inspired metaheuristic algorithm for global optimization problems. *Computers & Industrial Engineering*, 2021, vol. 158, p. 1–37. DOI: 10.1016/j.cie.2021.107408

[33] TITEL, F., BELATTAR, M. Optimization of NOMA downlink network parameters under harvesting energy strategy using multi-objective GWO. *Radioengineering*, 2023, vol. 32, no 4, p. 492–501. DOI: 10.13164/re.2023.0492

## About the Authors ...

**Faouzi TITEL** (corresponding author) received the Engineer degree in Electronics in 1995 from the University of Mentouri, Constantine, Algeria, the Magister degree in Electronics in 1998 from the University of Ferhat Abbas, Sétif, Algeria, and the Doctorate degree in Electronics from the University of Mentouri 1, Constantine, Algeria. He is currently an Associate Professor in the Department of Electronics, Electrical Engineering & Automation (EEA) of the National Polytechnic School of Constantine, Algeria. He becomes the head of the Automatic Control Specialty Team in 2021. He is also a member of the scientific committee of the department EEA. His research interests include optimization, multi-objective optimization, evolutionary algorithms, swarm intelligence techniques, intelligent control, NOMA, RIS, fuzzy inference systems, neuro-fuzzy systems, wavelet neural networks, nonlinear & multivariable systems, identification & control, embedded and real time systems, advanced technologies and application of wireless technologies.

**Mounir BELATTAR** received the diploma of Engineer in Electronics in 1993 from the University Mentouri 1 of Constantine and the diploma of Magister in 1996 from the same university. In 1996, he was teaching electrical circuits in Djelfa University, and from 1999 to 2012, he was a head and principal engineer of Electrical Development Networks Office in SONELGAZ factory. In 2012, he received the doctorate degree and joined Skikda University as a lecturer, where he was teaching microwave and radiofrequency circuits. Actually, he is a full professor at the University 20 Août 1955 Skikda. He is also the head of the master's telecommunication course, at the Department of Electrical Engineering, and a member the doctoral school. His main research interests are 5G/6G networks, wireless communication theory, non-orthogonal multiple access networks assisted by UAV communications and reconfigurable intelligent surfaces.

**Mohamed LASHAB** received the D.E.S. degree (higher degree of education in electronics) from Constantine University, Algeria, in 1988, the M.Phil. degree from Trent Polytechnic, Nottingham, England, in 1990, and the Ph.D. degree in 2009. He joined Skikda University, Algeria, as a Senior Lecturer, in 1995, where he was teaching electrical circuits and electromagnetic principles. He started working on reflector antennas in 2004, by using moment method combined with wavelets. Actually he is a professor in microwave structures at Larbi Ben M'hidi University, Oum El Bouaghi, Algeria. He becomes the head of the laboratory of research of Electronics and New Technologies (ENT) in 2020. His main research interests are horn antennas, planar antennas, electromagnetic sensors, and artificial materials such as meta-materials and chirals to improve antennas performance. He has published and co-authored more than 100 papers in scientific journals and conference proceeding since 2006. He is the member of editorial board of many journals, and the member of technical program committee/international advisory board/ international steering committee.

**Raed ABD-ALHAMEED** is a Professor of Electromagnetic and Radiofrequency Engineering with the University of Bradford, U.K. He is also the leader of radiofrequency, propagation, sensor design, and signal processing; in addition to leading the Communications Research Group for years within the School of Engineering and Informatics, University of Bradford. He has long years' research experience in the areas of radio frequency, signal processing, propagations, antennas, and electromagnetic computational techniques. He has published over 800 academic journals and conference papers; in addition, he has co-authored seven books and several book chapters including seven patents. He is a principal investigator for several funded applications to EPSRCs, Innovate UK and the leader of several successful knowledge Transfer Programs, such as with Arris (previously known as Pace plc), Yorkshire Water plc, Harvard Engineering plc, IETG Ltd., Seven Technologies Group, Emkay Ltd., and Two World Ltd. He has also been a co-investigator in several funded research projects including 1) H2020-MSCA-RISE-2024-2028; Marie Skłodowska-Curie, Research and Innovation Staff Exchange (RISE), titled: 6G Terahertz Communications for Future Heterogeneous Wireless Network; 2) HORIZON-MSCA-2021-SE-01-01, Type of Action: HORIZON-TMA-MSCA-SE 2023-2027: ROBUST: Proposal title: "Ubiquitous eHealth Solution for Fracture Orthopedic Rehabilitation"; 3) Horizon 2020 research and innovation program under grant agreement H2020-MSCA-RISE-2019-eBORDER-872878; 4) H2020 MARIE Skodowska-Curie ACTIONS: Innovative Training Networks Secure Network Coding for Next Generation Mobile Small Cells 5G-US; 5) European Space Agency: Satellite Network of Experts V, Work Item 2.6: Frequency selectivity in phase-only beamformed user terminal direct radiating arrays; 6) Nonlinear and demodulation mechanisms in biological tissue (Dept. of Health, Mobile Telecommunications & Health Research Program; and 7) Assessment of the Potential Direct Effects of Cellular Phones on the Nervous System (EU: collaboration with six other major research organizations across Europe). He was a recipient of the Business Innovation Award for his successful KTP with Pace and Datong companies on the design and implementation of MIMO sensor systems and antenna array design for service localizations. He is the chair of several successful workshops on energy-efficient and reconfigurable transceivers: Approach toward Energy Conservation and $CO_2$ Reduction that addresses the biggest challenges for future wireless systems. He is also the general chair of the IMDC-IST International Conference since 2020. He has been a co-editor for Electronics MDPI Journal since June 2019; in addition, he was a Guest Editor of IET Science, Measurements and Technology Journal since 2009. He has been a Research Visitor of Wrexham University, Wales, since 2009, covering the wireless and communications research areas. His interests are in computational methods and optimizations, wireless and mobile communications, sensor design, EMC, beam steering antennas, energy-efficient PAs, and RF predistorter design applications. He is a fellow of the Institution of Engineering and Technology, fellow of the Higher Education Academy and a Chartered Engineer.